

# Scanning droplet cell investigations on single grains of a FeAlCr light weight ferritic steel

Kirsten Agnes Lill, Achim Walter Hassel<sup>\*,1</sup>, Georg Frommeyer, Martin Stratmann<sup>1</sup>

*Max-Planck-Institut für Eisenforschung GmbH, Max-Planck-Str. 1, D-40237 Düsseldorf, Germany*

Received 29 March 2005; received in revised form 28 April 2005; accepted 16 May 2005

Available online 31 August 2005

In memoriam Joachim Walter Schultze (†2005.03.14)

## Abstract

Polycrystalline Fe7.5Al7Cr is a ferritic light weight steel that shows a strong anisotropic dissolution behaviour. This electrochemical phenomenon was investigated by use of a scanning droplet cell (SDC). The crystallographic orientation of the single grains was determined by electron back scatter diffraction (EBSD). The fraction of grains with a near  $\langle 111 \rangle$  orientation ( $<10^\circ$ ) was 1.88 times higher than that of the near  $\langle 001 \rangle$  orientation prior to annealing and 3.58 times higher after annealing. Voltammograms were performed on single grains with low index planes. The critical current density was 53% higher on  $\langle 001 \rangle$  grains as compared to  $\langle 111 \rangle$  grains. These results are used to discuss the electrochemical behaviour of the polycrystalline FeAlCr.

© 2005 Elsevier Ltd. All rights reserved.

**Keywords:** FeAlCr alloy; Single grains; Scanning droplet cell; EBSD

## 1. Introduction

Cost and weight reductions have always been a motivation for the development of new steels. The partial replacement of Cr with Al results in weight reduction and subsequently in lighter materials. FeAlCr alloys with Al- and Cr-contents between 6 and 8 wt% show promising mechanical properties, high yield strength and good deep-drawing capabilities.

The substitution of Cr with Al causes two effects which both result in a reduction of density. As shown in Fig. 1, the lower atomic weight of Al when compared to Cr yields in a density reduction. The ratio of the atomic weights of the three components Fe:Cr:Al is 55.847:51.996:26.981 as schematically represented by the lengths of the bars (Fig. 1). The second effect is a lattice expansion due to the larger radius of the Al atoms, displayed by the circles which represent the Goldschmidt radii in Fig. 1 being 143 pm for Al, 124 pm

for Fe and 124 pm for Cr. Only few investigations were performed on FeCrAl alloys with Cr- and Al-contents between 6 and 8 wt% [1,2].

The grain orientation-dependent electrochemical characteristics on polycrystalline material have been rarely investigated because of the absence of practical electrochemical methods with sufficient lateral resolution. The scanning droplet cell (SDC) offers the feasibility for electrochemical investigation with a sufficiently high lateral resolution [3–5]. Hassel [6], Lohrengel and Moehring [5] published results on the electrochemical behaviour of aluminium oxide films on aluminium grains and grain boundaries using the SDC. Dieckertmann et al. investigated the structure of the oxide on  $(100)$  and  $(111)$  oriented planes of gold single crystals. They assumed that the oxide structure is independent of orientation of the gold substrate [7]. Hassel and Seo performed capacity scans and potentiodynamic scans on coarse grain gold [8]. In an attempt to separate the influence of crystal orientation and grain boundary they performed experiments on polycrystalline gold samples with all grains being  $(111)$  oriented but azimuthally rotated. In

\* Corresponding author. Fax: +49 211 6792 218.

E-mail address: [hassel@elchem.de](mailto:hassel@elchem.de) (A.W. Hassel).

<sup>1</sup> ISE active member.

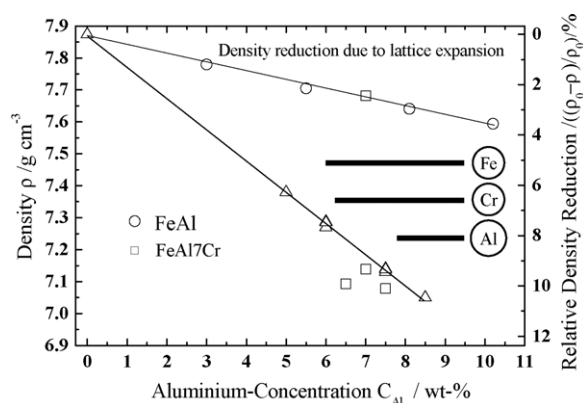


Fig. 1. Density and relative density reduction of binary Fe–Al alloys (○, △) in comparison to ternary Fe–Al–7Cr alloys (□).

these cases, the differences in the electrochemical behaviour such as capacity can be attributed to the grain boundaries themselves. Schultze et al. investigated the influence of grains and grain boundaries of titanium and iron on corrosion and passivation in nanoscopic and microscopic dimensions by means of photoresist microelectrodes. They showed that the density of surface atoms determines the ion transfer reactions (oxide film formation) as well as the rate of electron transfer reactions [9,10]. Park and Lohrengel investigated the grain-dependent passivation of surfaces of polycrystalline zinc [11]. They suggested that the oxide formation rate is larger on grains with higher surface packing density.

In the work presented here the effects of crystallographic grain orientation on the electrochemical behaviour of single grains in the polycrystalline ternary system Fe7.5Al7Cr were investigated. The SDC was employed in combination with EBSD.

## 2. Experimental

### 2.1. Chemicals

All solutions were prepared from p.a. grade chemicals and deionized water. A miniaturised AuHg/Hg<sub>2</sub>SO<sub>4</sub>/Na<sub>2</sub>SO<sub>4</sub> reference electrode was used. This electrode was fabricated based on the method described in [12,13]. Its potential was checked against a Hg/Hg<sub>2</sub>SO<sub>4</sub>/0.5 M H<sub>2</sub>SO<sub>4</sub> reference electrode which was previously calibrated versus a commercial type Ag/AgCl/3 M KCl reference electrode. A thin gold wire (Wieland Dental + Technik) with a diameter of 200 μm and a purity of 99.999% was used as counter electrode. The FeAlCr working electrodes with grain sizes between 10 and 80 μm were prepared in house. The chemical composition of the alloy is given in Table 1. The grains were further grown by annealing for 20 h at 900 °C under laboratory atmosphere. Grain sizes up to 300 μm had been achieved. The sample was ground with 600 and 1000 grid paper. The grinding process was followed by finalising with 3 μm- and 1 μm-diamond solution. The final step was a mixture of grinding and etching

Table 1  
Chemical composition of Fe7.5Al7Cr

Fe7.5Al7Cr	wt%
Al	7.47
C	0.0008
Cr	6.98
Mo	<0.01
N	0.0178
Nb	<0.01
O	0.071
P	<0.01
S	0.0017
Ti	<0.001
Fe	Balance

with an alkaline SiO<sub>2</sub>-slurry with a particle size of 250 nm. Between the individual steps the sample has been cleaned in deionized water, acetone and ethanol in an ultra sonic bath to remove residuals from the preparation processes. All potentials in the electrolyte are given versus the standard hydrogen electrode (SHE).

### 2.2. Electronic equipment

A PAR Potentiostat/Galvanostat Model 283 (Princeton Applied Research) was used for the electrochemical measurements. For an effective positioning of the capillary on the working electrode surface an xyz stage (Physik Instrumente) was used. It was driven by a four-channel precision dc-motor controller C-844 (Physik Instrumente). This controller was steered by a program written in Agilent VEE 6.0. To realise the fine volume control of the SDC a microsyringe injector in combination with a Micro Controller (World Precision Instruments) was used. In the injector a 100 μL microsyringe (SGE) was mounted. The microsyringe was connected to the electrolyte inlet of the scanning droplet cell. By the use of a multiple tube system a second manually controlled syringe with a 5 mL volume was used for flushing the cell before and after the measurements. The Micro Controller was also monitored by the control program.

### 2.3. Scanning droplet cell

A schematic view of the SDC is given in Fig. 2. The scanning droplet cell consists of a small capillary which has a sealing on its tip and can be positioned directly onto the sample surface. The inner diameter of the capillary defines the area of the working electrode to be investigated. The other end of the capillary is fixed in a plastic screw which is mounted in an acrylic block with four channels, which meet in the centre of the block. The gold wire counter electrode is stuck in a plastic screw with epoxy resin glue. The gold wire is then mounted in the acrylic block in such a way that the gold wire is positioned in the capillary. A μ-reference electrode (AuHg/Hg<sub>2</sub>SO<sub>4</sub>/Na<sub>2</sub>SO<sub>4</sub>) is fixed in a third screw and mounted in the acrylic block [12]. The fourth tube serves as electrolyte inlet. To seal the cell an o-ring gasket is fixed on

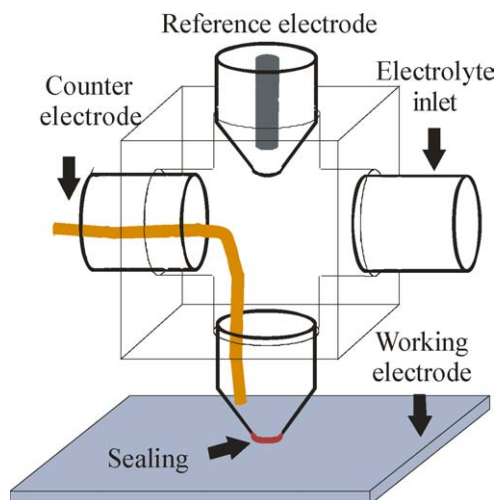


Fig. 2. Schematic view of the scanning droplet cell (reference electrode: Hg/Hg<sub>2</sub>SO<sub>4</sub>; counter electrode: Au-wire).

the tip of each screw. For rough positioning of the electrochemical cell onto the sample surface and into the camera focus the acrylic cell block is mounted to the manually controlled *xyz*-micromanipulator. For a fine positioning which allows the addressing of single grains a computer controlled *xyz*-positioning system was used. The positioning and the contact of the sealing to the sample surface could be observed using a long distance microscope. To control the electrolyte volume in the tip of the capillary a pl-syringe with a sufficiently high resolution to guarantee a continuous control of the droplet volume was used.

#### 2.4. Electrochemical cell for macroscopic investigations

Investigations on macroscopic samples ( $\varnothing = 6$  mm) were performed in an electrochemical cell that consisted of a double-walled glass cell with seven standard ground glass joints. The joints were used to connect working electrode, reference electrode, counter electrode and supplies for gas, electrolyte and rinsing water. A commercial type Ag/AgCl/3 M KCl reference electrode (Metrohm) and a gold counter electrode were used.

#### 2.5. Microprober

For addressing areas of interest on the samples a manual PM 5 Probe Station (Karl Süss) including a PH 150 Micro-manipulator (Karl Süss) and a microscope (Mitutoyo WF, magnification up to 1000 $\times$ ) has been used. The tip of the micromanipulator was equipped with a sharp steel scalpel to set markers for the EBSD investigations.

#### 2.6. Field emission-scanning electron microscopy (FE-SEM)

The SEM measurements were performed on a scanning electron microscope model 1550 VP from LEO, UK. An

acceleration voltage of 15 kV and a multi-pressure secondary electron (MPSE) detector were used.

#### 2.7. Electron back scatter diffraction (EBSD)

The before mentioned microscope was also equipped with an EBSD detector from TSL. The system includes a CCD camera digi view 12. The aperture used for the EBSD mapping was 60  $\mu\text{m}$ . The tilting angle of the sample stage was 63.5 $^\circ$ , acceleration voltage 20 kV and step size 3.2  $\mu\text{m}$ .

#### 2.8. Cyclic voltammetry

The cyclic voltammetric scans were recorded between  $-0.5$  and  $1.75$  V versus SHE at a rate of  $50 \text{ mV s}^{-1}$ . All measurements were carried out in  $0.5 \text{ M H}_2\text{SO}_4$ .

### 3. Results

#### 3.1. Macroscopic measurements

First, a potentiodynamic measurement was performed on a sample with a scan rate of  $dE/dt = 330 \mu\text{V s}^{-1}$  in  $0.5 \text{ M H}_2\text{SO}_4$ .

After the measurement the sample was thoroughly rinsed and dried. The sample surface displayed a high roughness. Further investigations were made with the SEM. Fig. 3 shows a scanning electron micrograph of the sample. The grain boundaries and the single grains can be clearly seen. The grains have sizes between 10 and 80  $\mu\text{m}$ . Significant differences in height are observed. This is attributed to a strong anisotropy of the dissolution rate. Thus, additional investigations were performed with the SDC in combination with EBSD to go into the details of the different electrochemical behaviour of the grains.

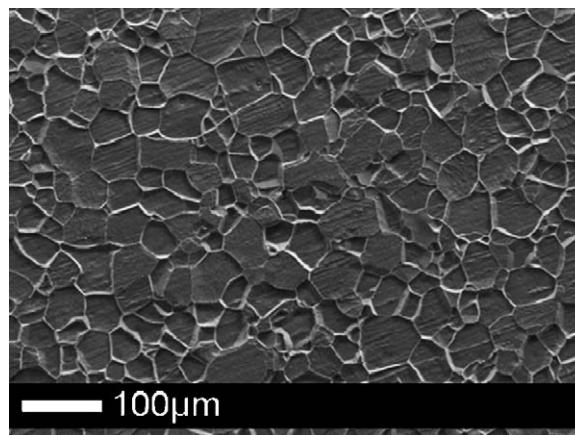


Fig. 3. Surface of polycrystalline alloy Fe7.5Al7Cr after potentiodynamic measurement in  $0.5 \text{ M H}_2\text{SO}_4$ ,  $dE/dt = 330 \mu\text{V s}^{-1}$ .

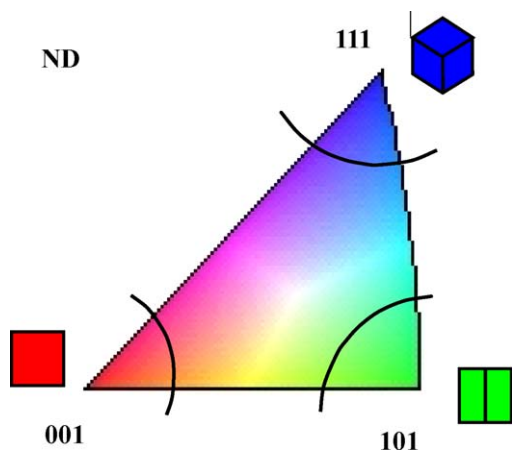


Fig. 4. Normal direction (ND) inverse pole figure for a ferritic material: the colour red is assigned to the  $\langle 001 \rangle$  crystal direction, green to  $\langle 101 \rangle$  and blue to  $\langle 111 \rangle$ .

### 3.2. EBSD mapping

Fig. 5 shows an EBSD map of a polished sample prior to annealing. An area of  $940 \mu\text{m} \times 940 \mu\text{m}$  was investigated. For a clearer illustration just the low index grains  $\langle 001 \rangle$ ,  $\langle 101 \rangle$  and  $\langle 111 \rangle$  were colour coded. The classification of the crystallography was performed based on a tilting of up to  $10^\circ$  from the elementary index planes. This is indicated by the circle sections in the inverse pole figure (Fig. 4). The fraction of the low index planes before annealing shows that the alloy has a preferred orientation of  $\langle 111 \rangle$ . The fraction of  $\langle 111 \rangle$  grains is 1.88 times higher than the fraction for  $\langle 001 \rangle$  oriented grains with respect to the surface area fraction.

In order to quantify the dissolution rate of single grains, it was necessary to further increase the grain size. This was achieved by annealing the sample. Fig. 6 shows the result of the EBSD mapping performed on a sample after the annealing process. As for the sample shown in Fig. 5 an area of  $940 \mu\text{m}$  in square was investigated. Grain sizes of up to  $300 \mu\text{m}$  were obtained. Even after the annealing process the fraction of  $\langle 111 \rangle$  grains remains predominant for the low index grains considered here. The fraction is 3.58 times higher than for the  $\langle 001 \rangle$  oriented grains. The absolute value of the  $\langle 101 \rangle$  oriented grains did not change. Grains from these low index planes were considered as representatives for the electrochemical experiments.

### 3.3. Scanning droplet cell

In order to characterise the electrochemical behaviour of single grains, cyclic voltammetry was individually performed on different grains with different orientations. The inner diameter of the capillary was  $70 \mu\text{m}$ . The investigated surface area was  $3.85 \times 10^{-5} \text{cm}^2$ . The real investigated areas are shown in Fig. 7 as small sections of Fig. 6. Fig. 7 shows the cyclic voltammograms on two different grains with the orientations of  $\langle 001 \rangle$  (red curve) and  $\langle 111 \rangle$  (blue curve)

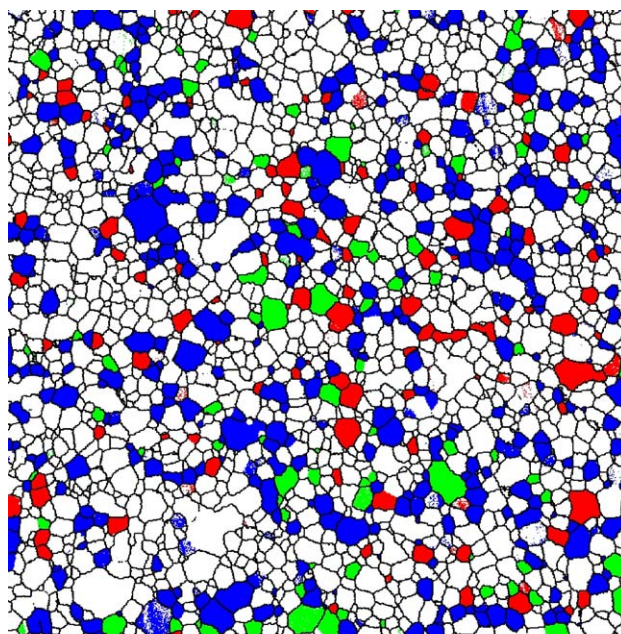


Fig. 5. EBSD map of a Fe7.5Al7Cr sample before annealing. The grain size is between  $10$  and  $80 \mu\text{m}$ . For reasons of clarity only grains with an orientation near ( $<10^\circ$ ) to the elementary planes  $\langle 100 \rangle$ ,  $\langle 110 \rangle$  and  $\langle 111 \rangle$  were colour coded.

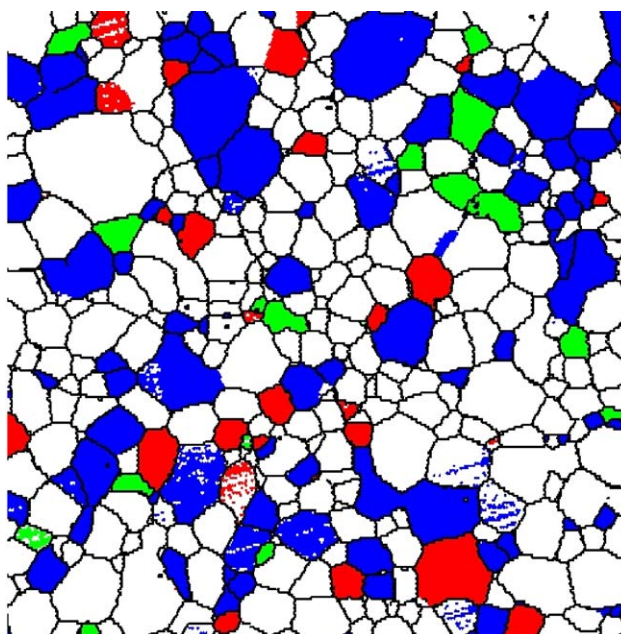


Fig. 6. EBSD map of a Fe7.5Al7Cr sample after annealing. The grain size ranges between  $50$  and  $200 \mu\text{m}$ . For electrochemical experiments, the low index planes were chosen as representatives. The classification of the crystallography was performed based on a deviation of up to  $10^\circ$  from the elementary index planes. This is indicated in the inverse pole figure by the circle sections Fig. 4.

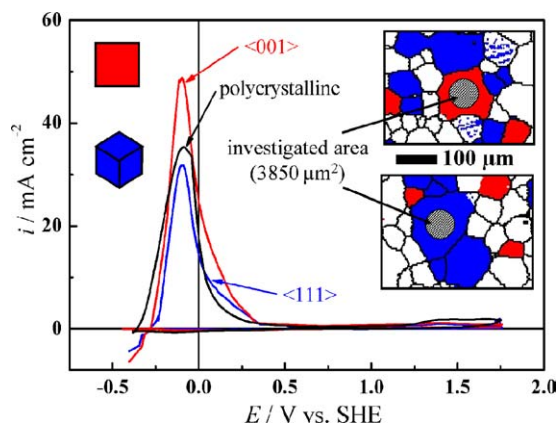


Fig. 7. Cyclic voltammograms obtained in  $\text{H}_2\text{SO}_4$  0.5M solution for Fe7.5Al7Cr single grains with orientation  $\langle 001 \rangle$  (red) and  $\langle 111 \rangle$  (blue) in comparison to polycrystalline measurements (black). Potential range  $-0.4$  to  $1.75$  V (vs. SHE),  $dE/dt = 50$   $\text{mV s}^{-1}$ .

Table 2

Critical current densities  $i_c$  and charge densities  $q$  for grains with orientations of  $\langle 001 \rangle$  and  $\langle 111 \rangle$  in comparison with results of measurements on polycrystalline material

Orientation	Critical current density, $i_c$ ( $\text{mA cm}^{-2}$ )	Charge density, $q$ ( $\text{C cm}^{-2}$ )
$\langle 001 \rangle$	48.65	0.223
$\langle 111 \rangle$	31.76	0.138
Polycrystalline	35.37	0.177

which had been recorded at a sweep rate of  $50$   $\text{mV s}^{-1}$ . Both voltammograms show a similar behaviour in the region of active to passive transition. The critical current density  $i_c$  for the  $\langle 001 \rangle$  oriented grain is 1.53 times higher than for the grain with  $\langle 111 \rangle$  orientation. The charge consumption  $q$  during the active to passive transition is 1.62 times higher for the  $\langle 001 \rangle$  oriented grain as compared to the grain with near  $\langle 111 \rangle$  orientation. For a better comparison of the results of the SDC measurements with the results obtained in the common electrochemical cell the values for the current densities have been calculated for a surface area of  $1$   $\text{cm}^2$ . The black curve in Fig. 7 represents the cyclic voltammogram performed in the common electrochemical cell. The polycrystalline area shows a similar electrochemical behaviour as the single grains. The critical current density  $i_c$  for the polycrystalline alloy lies between the critical current density  $i_c$  measured for the  $\langle 001 \rangle$  oriented grain and that measured for the grain with  $\langle 111 \rangle$  orientation. The charge consumption  $q$  during the passive to active transition presents equal characteristics. The exact values are given in Table 2.

#### 4. Discussion and summary

In this work the electrochemical behaviour of a polycrystalline FeAlCr alloy has been investigated. The alloy showed a significantly inhomogeneous performance in the electrochemical dissolution. This anisotropic behaviour led to an

unequal attack of the grains resulting in terraces of single grains. Further investigations were carried out on these single grains to exemplify the electrochemical behaviour of single grains by means of a SDC. Single grains with sizes down to  $150$   $\mu\text{m}$  were investigated, with the method having potential for further downsizing.

Grains of known crystallographic orientation were addressed by the SDC and cyclic voltammetry was performed. The  $\langle 001 \rangle$  grains showed significantly higher critical current densities  $i_c$  and charge consumptions  $q$  during the active to passive transition than those of  $\langle 111 \rangle$  orientation. On the other hand, the packing of atoms in the  $\langle 111 \rangle$  orientation is approximately 1.2 times higher than in the  $\langle 001 \rangle$  orientation. This discrepancy can be explained by the assumption, that the lower packing in the  $\langle 001 \rangle$  orientation enables the availability of the atom layer beneath the surface atom layer for interaction, which is more difficult for the  $\langle 111 \rangle$  orientation because of the denser packing. The involvement of the second  $\langle 001 \rangle$  layer to the packing density inverts the value, that the packing of the atoms in the  $\langle 001 \rangle$  orientation becomes approximately 1.7 times higher than that for the  $\langle 111 \rangle$  orientation. The difference in the value of the packing density to the values of  $i_c$  and  $q$  can be explained by the assumption that not all atoms of the second layer in the  $\langle 001 \rangle$  orientation take part in the interactions. Further investigations which are presently in progress shall clarify to which extend a higher dissolution rate of the open  $\langle 100 \rangle$  package is responsible and to which extend the formation of a passive film is involved in the observed charge consumption. EBSD maps showed the higher share of  $\langle 111 \rangle$  grains as compared to  $\langle 001 \rangle$  and  $\langle 101 \rangle$ . These findings were consistent with the fact that  $i_c$  and the charge consumed on polycrystalline material were closer to that of the  $\langle 111 \rangle$  grains.

To get a better understanding about how the behaviour of polycrystalline material is related to that of single grains further investigations have to be made, including electrochemical surface scans with the SDC as well as on single grains and on the grain boundaries.

A fully analytical description of the dissolution behaviour of polycrystalline material however requires more knowledge. In specific, it is necessary to:

- investigate a larger number of different crystallographic orientations;
- use a classification covering all represented crystallographic orientations;
- study the influence of the grain size on the dissolution kinetics;
- evaluate the contribution of the grain boundaries;
- investigate type and degree of interaction between adjacent grains.

Based on all these investigations, it should become possible to predict the overall electrochemical behaviour of polycrystalline material as a synthesis of all increments.

## Acknowledgement

Thanks are due to K.S. Tan for supporting the EBSD measurements.

## References

- [1] P.D. Hodgson, *Met. Forum* 7 (1984) 46.
- [2] K. Hio, *Corrosion (Houston)* 55 (1999) 822.
- [3] A.W. Hassel, M.M. Lohrengel, *Electrochim. Acta* 42 (1997) 3327.
- [4] M.M. Lohrengel, *Electrochim. Acta* 47 (2001) 137.
- [5] M.M. Lohrengel, A. Moehring, in: J. Walter Schultze, T. Osaka, M. Datta (Eds.), *Electrochemical Microsystem Technologies*, Taylor and Francis, New York, 2002, ISBN 0-415-27355-2.
- [6] A.W. Hassel, *Doctoral Thesis*, Verlag Shaker, Aachen, 1997, ISBN 3-8265-2981-2.
- [7] D. Dieckertmann, J.W. Schultze, K.J. Vetter, *Electroanal. Chem.* 55 (1974) 429.
- [8] A.W. Hassel, M. Seo, *Electrochim. Acta* 44 (1999) 3769.
- [9] J.W. Schultze, *Surf. Coat. Technol.* 169–170 (2003) 85.
- [10] J.W. Schultze, *Corros. Eng. Sci. Technol.* 39 (2004) 45.
- [11] C.J. Park, M.M. Lohrengel, *Electrochim. Acta* 47 (2002) 3395.
- [12] A.W. Hassel, K. Fushimi, M. Seo, *Electrochem. Commun.* 1 (1999) 180.
- [13] K.A. Lill, A.W. Hassel, *Electrochim. Acta*, submitted for publication.